DARPA/ONR Grant #N00014-91-J-1976

First Quarterly Progress Report
(covering the period of August 1 - October 31, 1991)

Project Title: Development of Ultra-Low Noise, High Sensitivity Planar Metal Grating Coupled AlGaAs/GaAs Multiquantum Well Detectors for Focal Plane Array (FPA) Staring IR Sensor Systems

Submitted to

Max N. Yoder
Office of Naval Research
Code 1114 SS
800 North Quincy Street
Arlington, VA 22217-5000

prepared by

Sheng S. Li, Professor
Dept. of Electrical Engineering
University of Florida
Gainesville, FL 32611
Tel.(904)-392-4937
Fax (904)-392-8671

November 1, 1991

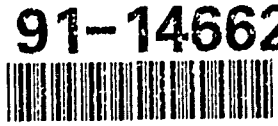

Quarterly Progress Report
(covering the period of August 1 - October 31, 1991)

DARPA IR Detector Contract under Navy Grant #NOO14-91-J-1976

Project Title: Development of Ultra-Low Noise, High Sensitivity Planar Metal Grating Coupled AlGaAs/GaAs Multiple Quantum Well Detectors for Focal Plane (FPA) Staring IR Sensor Systems

I. INTRODUCTION

Since the beginning of this DARPA sponsored IR detector project, we have made significant progress toward achieving the original project goals. We have designed and fabricated two new types of IR detectors using step- bound-to-miniband (SBTM) and bound-to-miniband (BTM) transition multiple-quantum-well (MQW)/superlattice (SL) barrier structures grown by MBE technique. The SBTM IR detector uses a slightly strained $In_{0.07}Ga_{0.93}As$ quantum well with short-period $Al_{0.4}Ga_{0.6}As/GaAs$ superlattice barrier grown on a GaAs substrate, and the BTM IR detector uses an enlarged $In_{0.47}Ga_{0.53}As$ quantum well with short-period superlattice $In_{0.48}Al_{0.52}As/In_{0.47}Ga_{0.53}As$ barrier grown on an InP substrate. The results showed that the dark current for the SBTM IR detector measured at 77 K was more than one order of magnitude lower than the conventional QWIP's (using bound-to-continuum band transition) reported in the literature. The detectivity for the SBTM IR detector structure measured at 50 ° light incident angle was found to be $2.1 \times 10^{10}\ cm\sqrt{Hz}/W$ at $V_b = 5$ V and T = 63 K. The other (BTM) IR detector structure showed a largely enhanced intersubband absorption at 10.73 μm (demonstrated for the first time) and a reduction of dark current by three orders of magnitude over the conventional LWIP's. To optimize the grating couplers for the top and back illumination, we have designed and fabricated 10 new photomasks with various grating patterns and different grating periodicities to be used for the proposed study of light coupling efficiency versus grating periodicity in the large area MQW/SL IR detectors. Specific accomplishments during this period are summarized as follows:

- Developed the first grating coupling AlGaAs/GaAs MQW/SL IR detector using bound-to-miniband (BTM) transition, and achieved a detectivity $D^* = 1.6 \times 10^{10} cm\sqrt{Hz}/W$ at $\lambda = 8.9$ μm and T = 77 K.

- Performed a systematic study of planar metal grating couplers with grating periods of $\Lambda = 1.1$, 3.2, 5, and 7.2 μm on this MQW IR detector under normal illumination. Detector with a quantum efficiency as high as 21.7% has been achieved by using a 5 μm surface grating coupler. Further improvement in the light coupling efficiency can be expected by optimizing the grating parameters.

- Designed and fabricated 10 new photomasks with various grating patterns and different metal grating periodicities. These photomasks will be used in our new MQW/SL IR detectors for front ohmic contacts and light coupling.

- Designed and fabricated a new low-dark current, high detectivity *step-bound-to-miniband* (SBTM) IR detector structure by using a slightly strained InGaAs quantum well with short-period superlattice GaAs/AlGaAs barrier. More than one order of magnitude reduction in the dark current has been obtained in this detector. The detectivity for this new IR detector was found to be $2.1 \times 10^{10}\ cm\sqrt{Hz}/W$ at $V_b = 5$ V and T = 63 K.

- Designed and grown a new bound-to-miniband (BTM) transition InGaAs quantum well with short-period superlattice InAlAs/InGaAs barrier grown on an InP substrate. A strong intersubband IR absorption at T = 300 K and $\lambda = 10.73\ \mu m$ has been observed for the first time in this structure. An integrated optical absorption strength of $I_A = 19.5$ Abs-cm$_{-1}$ was obtained at the Brewster's angle $\theta_B = 74.5°$ and at T = 300 K, which is about five times larger than that of the conventional single bound-to-bound transition. The results clearly show that the enlarged quantum well and broad miniband are superior for large infrared absorption and detection.

- A paper, entitled,"A metal grating coupled bound-to-miniband transition GaAs Mulitple Quantum Well/superlattice infrared detector," has been published in Appl. Phys. Lett., 59 (11), pp.1332-34, Sept.9, 1991.

- A paper entitled, "Largely enhanced bound-to-miniband absorption in an InGaAs multiple quantum well with short-period superlattice InAlAs/InGaAs barrier," accepted for publication in Appl. Phys. Lett., 59 (21), 18 November,1991.

- A paper entitled, "A low dark current step-bound-to-miniband absorption InGaAs/GaAs /AlGaAs multiple quantum well infrared detector," submitted to Appl. Phys. Lett., October 22, 1991.

- An abstract, entitled"Largely enhanced intersubband absorption in a wide InAlAs /InGaAs quantum well and short period superlattice," submitted to the *SPIE'S 1992 SYMPOSIUM on Quantum Wells and Superlattices*, Somerset, NJ, 23-27 March,1992.

- An abstract, entitled"Grating coupled bound-to-miniband III-V quantum well /superlattice barrier infrared detectors," submitted to *the conference on Infrared Detectors and Focal Plane Arrays at OE/Aerospace Sensing 92,*" Orlando, FL, April 20-24,1992.

II. COMPARISON OF DARK CURRENT MEASUREMENTS IN QWIPs

In this section we compare the results of dark current measurements made on four different types of quantum-well infrared photodetectors (QWIPs) fabricated during this reporting period. To facilitate our study of the performance of various QWIPs, we have designed and fabricated four different types of III-V QWIPs grown by MBE technique. Figure 1 shows the energy band diagrams of these four different types of QWIPs: Fig.1 (a) is a conventional bound-to-continuum band (BTCB) transition AlGaAs/GaAs (480/40 Å) multiquantum well infrared (IR) photodetector, (b) a bound-to-miniband (BTM) transition GaAs (88

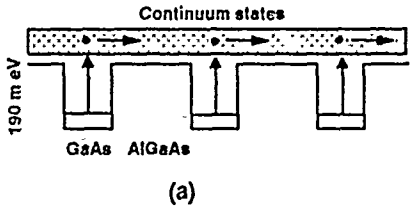

(a)

(a) The energy band diagram for a conventional AlGaAs/GaAs(480/40A) quantum well infrared photodetector (QWIP) with bound-to-continuum state transition.

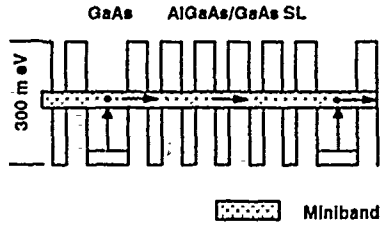

(b)

(b) The energy band diagram for an GaAs(88Å QW)/AlGaAs-GaAs(58-29A SL) QWIP with bound-to-miniband transition.

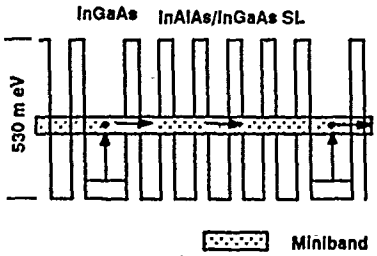

(c)

(c) The energy band diagram for an InGaAs (110A QW)/AlInAs-InGaAs(30-46A SL) QWIP Grown on InP substrate with bound-to-miniband transition.

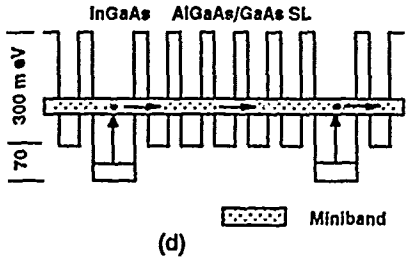

(d)

(d) The energy band diagram for an InGaAs(106A QW)/AlGaAs-GaAs(30-59A SL) QWIP with step-bound-to-miniband transition.

Figure.1 Energy band diagrams for four different types of III-V quantum well infrared photodetectors (QWIPs)

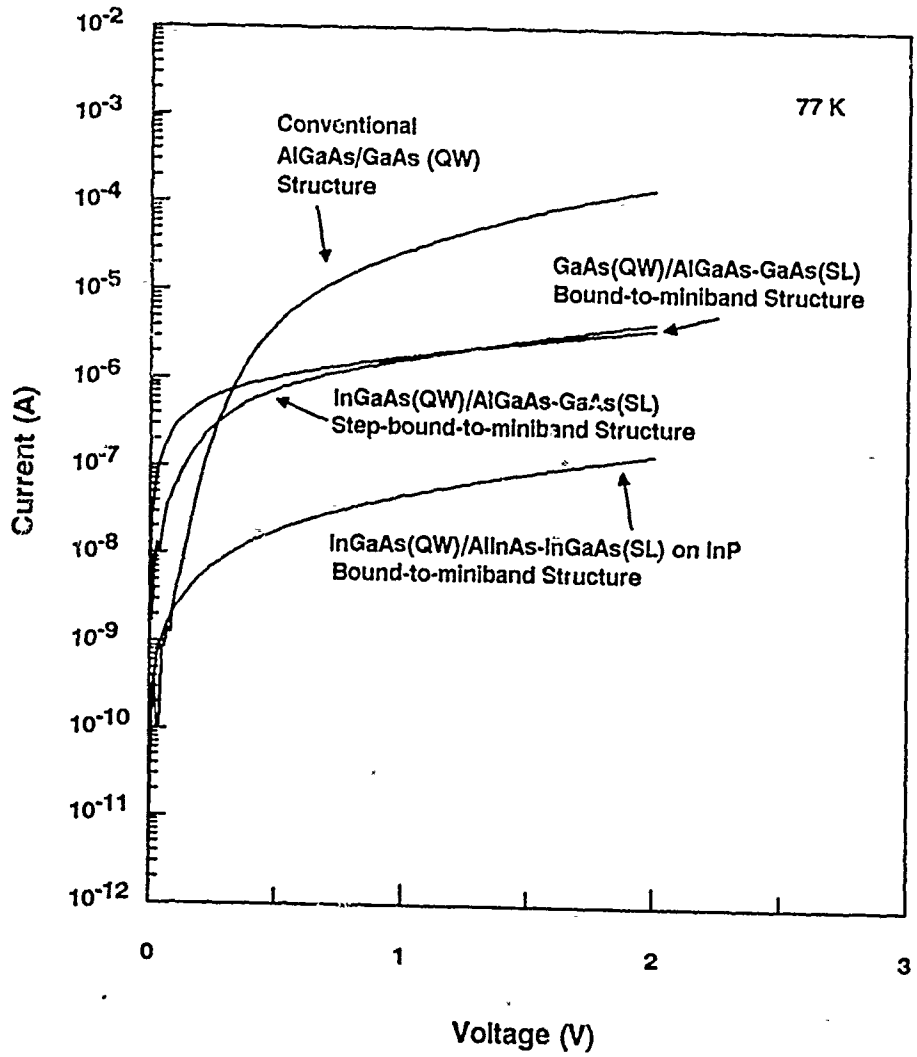

Figure.2 Dark current versus bias voltage for four different QWIPs shown in Fig.1, measured at 77 K.

Å) quantum well/AlGaAs-GaAs (58/29 Å) superlattice barrier IR detector, (c) a bound-to-miniband (BTM) transition InGaAs quantum well (110 Å)/InAlAs-InGaAs superlattice barrier structure grown on an InP substrate, and (d) a step-bound-to-miniband (SBTM) transition slightly strained InGaAs quantum well(106 Å)/AlGaAs-GaAs (30/59 Å) superlattice barrier structure grown on a GaAs substrate. The barrier heights for structures (a), (b), (c), and (d) are given by 190, 300, 530, and 370 meV, respectively. The dark currents measured at 77 K as a function of bias voltage are shown in Figure 2. The results showed that the dark currents for our (BTM) and (SBTM) QWIPs shown in Fig.1 (b) through Fig.1 (d) measured at V_b = 2 V and T = 77 K were two to three orders of magnitude lower than the conventional QWIP's shown in Fig.1 (a). Since the dark current in these QWIPs is dominated by the thermionic emission at 77 K, the results are consistent with the theoretical prediction (i.e., the therminoic emission current depends exponentially on the barrier height in the quantum well). Detailed description and assessment of the performance characteristics for these new QWIPs (Fig.1 (b) - (d)) are given in Section IV.

III. INTERACTION WITH INDUSTRIAL LABORATORIES

In this IR detector project we have put our emphasis on establishing collaborations with researchers in industrial laboratories who are interested in the long wavelength III-V quantum-well infrared detectors grown by MBE technique. The research team at the University of Florida consists of Dr. Li, the principal investigator, and four of his graduate students who are working on their Ph.D. research in IR detector project. All the quantum well/superlattice IR detectors are designed, fabricated and characterized by our group in the microelectronics laboratory of the Electrical Engineering Department of the University of Florida. Dr. Pin Ho of the Electronics Laboratory of General Electric Co. has helped us growing the InGaAs/GaAs/AlGaAs and other quantum well/superlattice layer structures by MBE technique. The collaboration enables us to make rapid progress in our IR detector project. We anticipate this collaboration to continue for the coming year and beyond. We have also exchanged the prepublication information on the IR detector papers with Dr. Barry Levine of A T & T Bell Laboratories. And Dr. Li plan to visit Dr. Levine's laboratories in March, 1992. Collaboration with these people will definitely benefit greatly to our ongoing IR detector research.

IV. TECHNICAL RESULTS

4.1. A Low Dark Current Step-Bound-to-Miniband Transition InGaAs/GaAs/AlGaAs Multiquantum Well Infrared Detector

The possibility of realizing novel high-speed quantum well devices such as lasers, photodetectors, and modulators has spurred extensive investigations on the intersubband absorption in quantum wells and superlattices[1-9]. A great deal of work has been reported on the lattice-matched GaAs/AlGaAs[10-14] and InGaAs/InAlAs/InP[15-17] quantum well systems. Recent studies[13,16] revealed that 8 - 12 μm infrared detectors may be obtained by using a multi-quantum well(MQW)/superlattice (SL) barrier structure and resonant tunneling mechanism. A significant improvement in intersubband absorption and thermionic emission property

has been successfully demonstrated using GaAs/AlGaAs superlattice reinforced bound-to-miniband (BTM) transition[8,14] structure. The replacement of bulk barrier region with a very short period superlattice barrier layer offers several new properties such as reduction of interface recombination, elimination of deep level related phenomena[18], realization of a new type of quantum photocurrent gain ($\sim 10^4$)[9,19], and a significant enhancement of intersubband absorption[16].

In this letter we report an ultra-low dark current lightly-strained InGaAs/GaAs/AlGaAs QWIP's based on the step-bound-to-miniband (SBTM) transition, superlattice miniband resonant tunneling and coherent transport mechanism. As illustrated in figure 1, the transition scheme of our QWIP's is from the localized bound ground state in the enlarged $In_{0.07}Ga_{0.93}As$ quantum wells to the resonant-coupled miniband of GaAs/ $Al_{0.4}Ga_{0.6}As$ superlattice (SL) barrier. This new structure created a potential 'step' in the superlattice barrier region to block the undesirable tunneling dark current from the heavily doped ground state E_{EW} in the quantum well. The physical parameters of the quantum wells and superlattices are chosen so that the ground bound state in the enlarged (EW) InGaAs well is pushed below the step barrier, and the first excited level E_{EW_1} of the quantum well is merged and lined up with the ground level of the miniband E_{SL} in the superlattice barrier layer to achieve a large oscillation strength f and intersubband absorption coefficient α[8,16]. Since the superlattice has a relatively thin barrier, the photoexcited electrons can easily tunnel through the superlattice barrier layer and transport along the aligned miniband, which are then collected by the external ohmic contacts.

To characterize the SBTM transition we performed theoretical calculations of the energy states E_{EW}, E_{SL} and the transmission coefficient T^*T on our LWIP's by using the multiple-layer transfer matrix method[8], and the results are shown in figure 2. It is noted that a broad and strongly degenerated miniband E_{SL} was formed inside the enlarged well by using the superlattice barrier structure. The ground state of the enlarged InGaAs well is confined much below the step barrier height so as to reduce the sequential tunneling and hopping currents. As a comparison, in the inset of figure 2, we calculated the transmission coeffecient of the superlattice for both the step-bound-to-miniband (SBTM) transition structure and the normal bound-to-miniband (BTM) transition structure without the potential step. Many orders of magnitude reduction in T^*T were observed in the present SBTM structure.

The SBTM detector structure was grown on a semi-insulating (S.I.) GaAs substrate by using the molecular beam epitaxy (MBE) technique. A 1 μm thick GaAs buffer layer of 1.4×10^{18} cm^{-3} was first grown on a S.I. GaAs substrate, followed by the growth of a 40-period of $In_{0.07}Ga_{0.93}As$ quantum wells with a well width of 106 Å and a dopant density of 1.4×10^{18} cm^{-3}. The barrier layer on each side of the quantum well consists of a 5-period of undoped $Al_{0.4}Ga_{0.6}As$ (30 Å) /GaAs (59 Å) superlattice layers which were grown alternatively with the InGaAs quantum wells. Finally, an n^+-GaAs cap layer of 0.4 μm thick and dopant density of 1.4×10^{18} cm^{-3} was grown on top of the MQW/SL layer structure to facilitate ohmic contacts. An array of 200×200 μm^2 mesas were chemically etched down to n^+-GaAs buffer contact layer on the GaAs substrate. Finally, AuGe/Ni/Au ohmic contacts were evaporated onto the top and bottom of n^+-GaAs contact layers by using E-

beam evaporation.

Device characterization was performed in a liquid-helium cryogenic dewar. An HP4140B semiconductor parameter analyzer was used to measure the dark current vs. voltage (I-V) curves. Under dark conditions, electrons can transfer out of the quantum wells and produce the observed current mainly via two mechanisms. One is attributed to the thermionic emission out of the quantum wells, which is the dominant current component at higher temperatures (i.e., for $T \geq 77$ K). The other is the thermally generated carriers tunneling through the superlattice miniband. In the present SBTM transition structure, we created a levitated potential step in the superlattice to block much of the tunneling current component due to electron tunneling from the heavily populated ground state at low temperatures. We also chose a high value of 'Al' composition, $x = 0.4$, which gave rise to a barrier potential as high as $\Delta E_c \simeq 388$ meV ($\sim 65\% \Delta E_g$), to suppress the thermionic emission out of the quantum wells. Figure 3 shows the measured dark I-V curves for temperatures between 35 and 92 K. Substantial reduction in device dark current was achieved in the present step-potential reinforced InGaAs multiquantum well/GaAs/AlGaAs superlattice barrier structure. To identify the origins of the dark currents flow in the detector we performed the numerical calculation of the dark currents using the expression[10,20]

$$I_D = \frac{4\pi q A v(\mathcal{E}) m^* kT}{h^2 L} \int_0^\infty |T(E,\mathcal{E})|^2 \{ln[1 + e^{-(E-E_f)/kT}] - ln[1 + e^{-(E-qV-E_f)/kT}]\} dE; \quad (1)$$

where $v(\mathcal{E})$ is the electron velocity in GaAs which is given by[21]

$$v(\mathcal{E}) = \frac{\mu\mathcal{E} + v_s(\mathcal{E}/\mathcal{E}_0)^4}{1 + (\mathcal{E}/\mathcal{E}_0)^4} \quad (2)$$

where q is the electron charge, A is the device area, m^* is the electron effective mass, L is the multiquantum well period, E_f is the Fermi level, $\mathcal{E}_0$ is the critical field which is equal to 4×10^3 V/cm for GaAs. As previously described[8], the parameter $|T(E,\mathcal{E})|^2$ is the field-dependent transmission coefficient which can be calculated by using the multi-layer matrix method, assuming the potential energy variation of $V(x) = V_0 + q\mathcal{E}x$. The calculated current values are in good agreement with the observed results, which shows that the levitated step potential barrier is indeed very effective in suppressing the device dark current. Another interesting result observed in this SBTM LWIP's (as shown in figure 3) is that the negative resistance exhibited by the sequential resonant tunneling through an expanding high-field superlattice domain[3] at T = 35 K.

Measurement of the intersubband absorption for the present detector was performed at 300 K using a Perkin-Elmer Fourier transform infrared (FTIR) spectroscopy. Figure 4 shows the room temperature absorption spectra at the Brewster's angle ($\theta_B = 73°$). The measured peak absorbance $A = -\log_{10}$ [transmission] was found to be about 40 mAbs. The absorption peak is centered at 11.4 μm. The full width at half-maximum (FWHM) of the absorption peak is about 220 cm^{-1}. To determine the spectral responsivity, the edge of the sample was polished into 50° to facilitate light illumination. The photocurrent was measured using a CVI Laser Digikrom 210 monochromator and an ORIEL ceramic element infrared source.

The responsivity R_λ = 0.38 A/W was obtained at V_b = 5 V and T = 77 K. Figure 5 shows the normalized responsivity versus wavelength measured at 77 K. From the measured responsivity and dark current, we can calculate the detectivity D^* of the detector using the relation

$$D^*_\lambda = R_\lambda (A\Delta f)^{1/2}/(4qI_dG\Delta f)^{1/2} \quad (3)$$

where A = 4×10^{-4} cm^2 is the effective area of the detector, G is the optical gain which is taken as 0.5[4]. At V_b = 5 V, we found that values of the peak detectivity at λ = 10.5 μm are D^* = 0.81×10^{10} and 2.1×10^{10} cm$\sqrt{Hz}$/W for T = 77 and 63 K, respectively.

In conclusion, we have demonstrated a new step-bound-to-miniband (SBTM) transition LWIP's using a lightly-strained InGaAs multiquantum well and a GaAs/AlGaAs superlattice barrier layer structure and resonant tunneling mechanisms. The new structure provided a levitated potential step in the superlattice barrier to block much of the tunneling current component from the heavily populated ground state in the quantum wells, which resulted in a significant reduction of the device dark current. The peak detectivity was found to be $D^* = 2.1 \times 10^{10} cm\sqrt{Hz}/W$ at λ = 10.5 μm and T = 63 K. With high detectivity and uniformity, this new SBTM LWIP's can be used for a wide variety of long wavelength (e.g., 8 – 12 μm) infrared applications.

REFERENCES

1. J. S. Smith, L. C. Chiu, S. Margalit, A. Yariv, and A. Y. Cho, J. Vac. Sci. Technol. B 1, 376 (1983).

2. L. C. West and S. J. Enlash, Appl. Phys. Lett. 46, 1156 (1985).

3. K. K. Choi, B. F. Levine, R. J. Malik, J. Walker, and C.G. Bethea, Phys. Rev. B 35, 4172 (1987).

4. B.F. Levine, G. Hasnain, C.G. Bethea, and Naresh Chand, Appl. Phys. Lett. 54, 2704 (1989).

5. S.D. Gunapala, B.F. Levine, R.A. Logan, T. Tanbun-Ek, and D.A. Humphrey, Appl. Phys. Lett., 57, 1802 (1990).

6. A. Kastalsky, T. Duffield, S.J. Allen, and J. Harbison, Appl. Phys. Lett. 52, 1320 (1988).

7. P.F. Yuh and K.L. Wang, Appl.Phys. Lett. 65, 4377 (1989).

8. Larry S. Yu, Sheng S. Li, Y.C. Kao, *Proc. Government Microcircuit Applications Conference*, Nov. 6 -8, Las Vegas, p.479 (1990).

9. S. S. Li, Y.H. Wang, Larry S. Yu, S. Zhu, R. M. Park and Y.W. Lin *International Electron Devices and Materials Symposium*, Nov. 14 -16, Hsinchu, Taiwan (1990).

10. B. F. Levine, C.G. Bethea, G. Hasnain, V O. Shen, E.Pelve, R.R. Abbott, and S.J. Hsieh, Appl. Phys. Lett. 56, 851 (1990).

11. G. Hasnain, B.F. Levine, S. Gunapala, and Naresh Chand, Appl. Phys. Lett. 57, 605 (1990).

12. K.W. Gossen and S.A. Lyon, Appl. Phys. Lett., 53. 1027 (1988).

13. Larry. S. Yu, S. S. Li, Y. C. Kao, *Proc. International Electron Devices and Materials Symposium*, Nov.14 -16, Hsinchu, Taiwan, p. 468 (1990).

14. Larry.S. Yu and Sheng S. Li, Appl. Phys. Lett. 59, 1332 (1991).

15. B.F. Levine, A.Y. Cho, J. Walker, R.J. Malik, D.A. Kleinman, and D.L. Sivco, Appl. Phys. Lett., 52, 1481 (1988).

16. Larry S. Yu, Sheng S. Li, and Pin Ho, Appl. Phys. Lett. Nov. 18 issue, (1991).

17. Hiromitsu Asai and Yuichi Kawamura, Appl. Phys. Lett., 56, 746 (1990).

18. H. Sakaki, M. Tsuchiya, and J. Yoshino, Appl. Phys. Lett., 47, 295 (1985).

19. F. Capasso, K. Mohammed, A.Y. Cho, R. Hull, A.L. Hutchinson, Appl. Phys. Lett. 47, 420 (1985).

20. R. Tsu and L. Esaki, Appl. Phys. Lett. 22 562 (1973).

21. S.M. Sze, *High-Speed semiconductor Devices*, John Wiley & Sons, pp. 60 (1990).

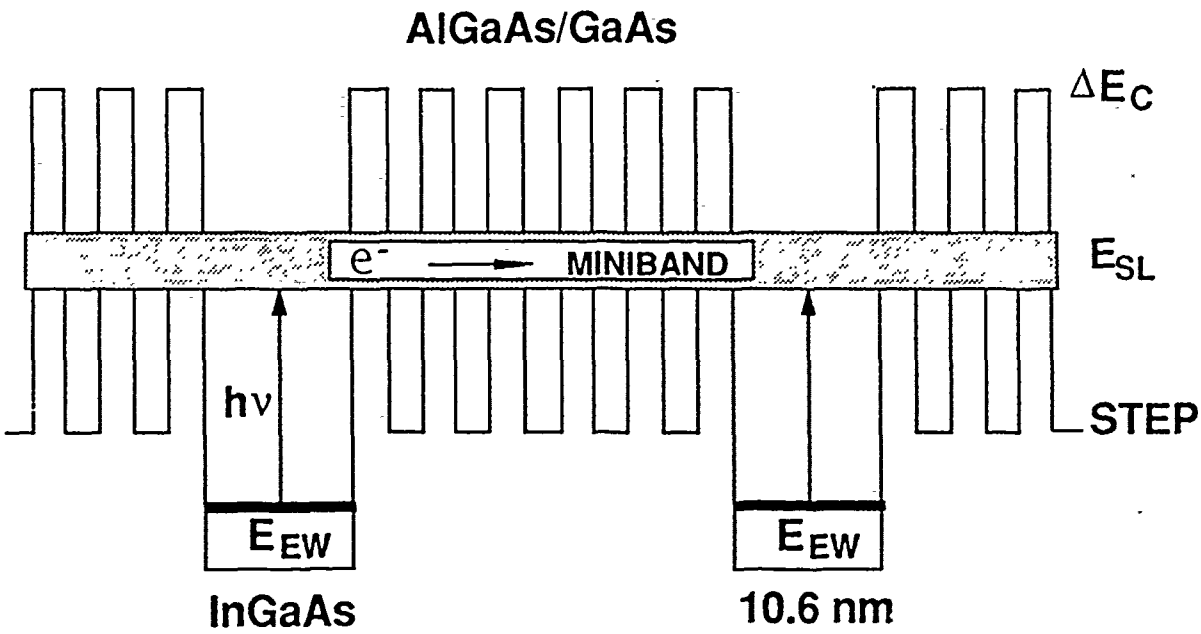

Figure.1 Energy band diagram for a step-bound-to-miniband (SBTM) transition InGaAs quantum well/AlGaAs-GaAs superlattice barrier infrared (IR) photodetector

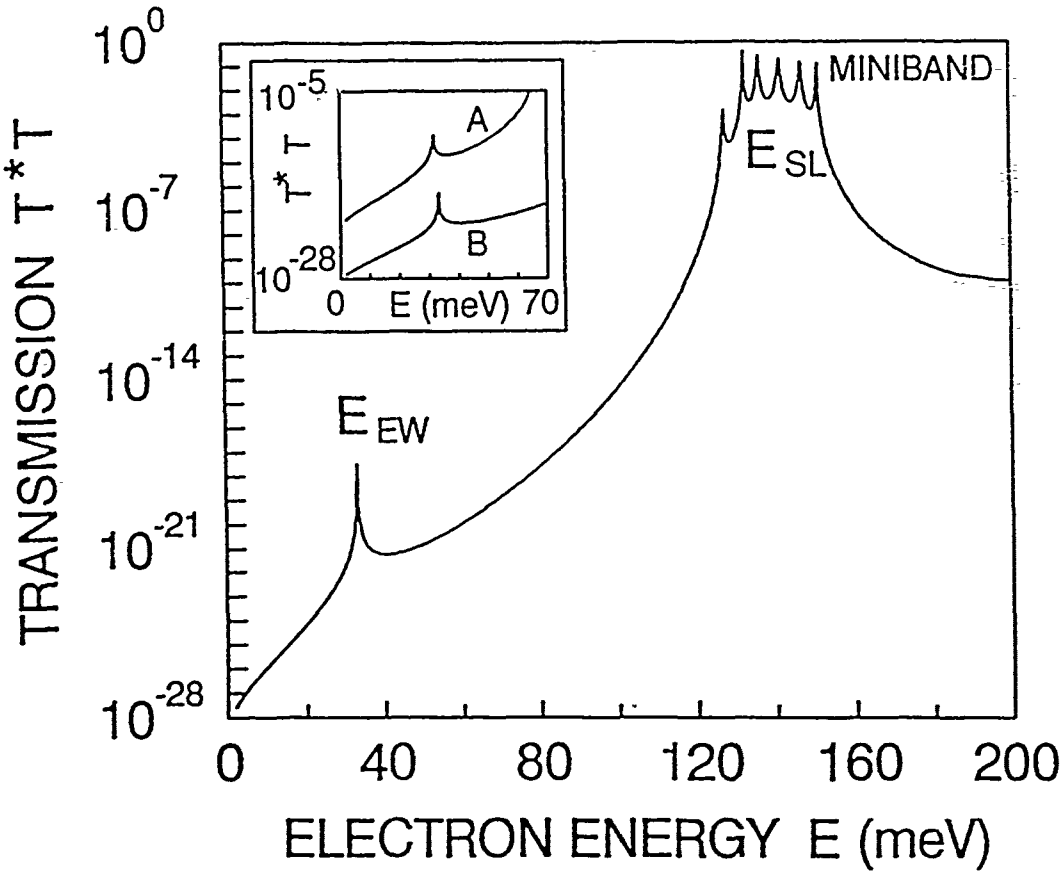

Figure.2 The calculated quantized energy states and transmission coefficient T*T for the SBTM IR detector shown in Fig.1. Inset: The calculated T*T ; curve A: BTM IR detector, curve B: SBTM detector structure.

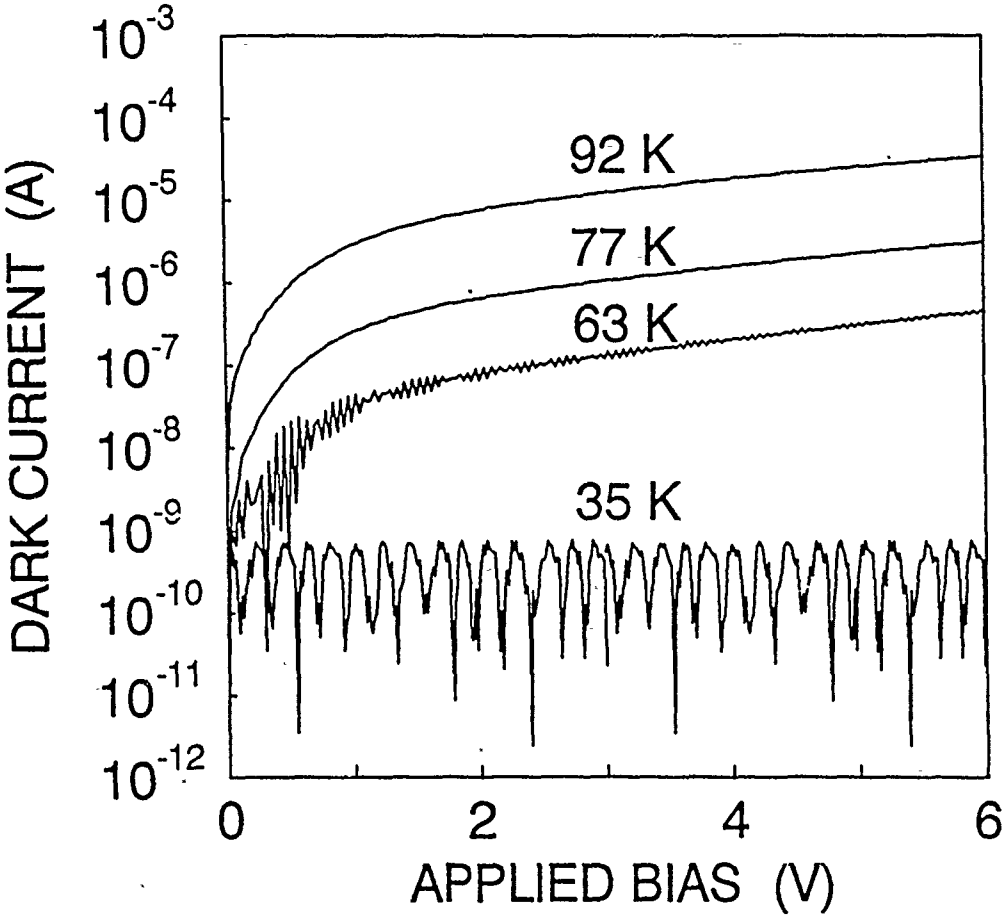

Figure.3 Dark current versus bias voltage for the SBTM IR detector shown in Fig. 1 for 35 < T <92 K. The dark current is dominated by thermionic emission for T >77 K, and by sequential tunneling for T < 35 K.

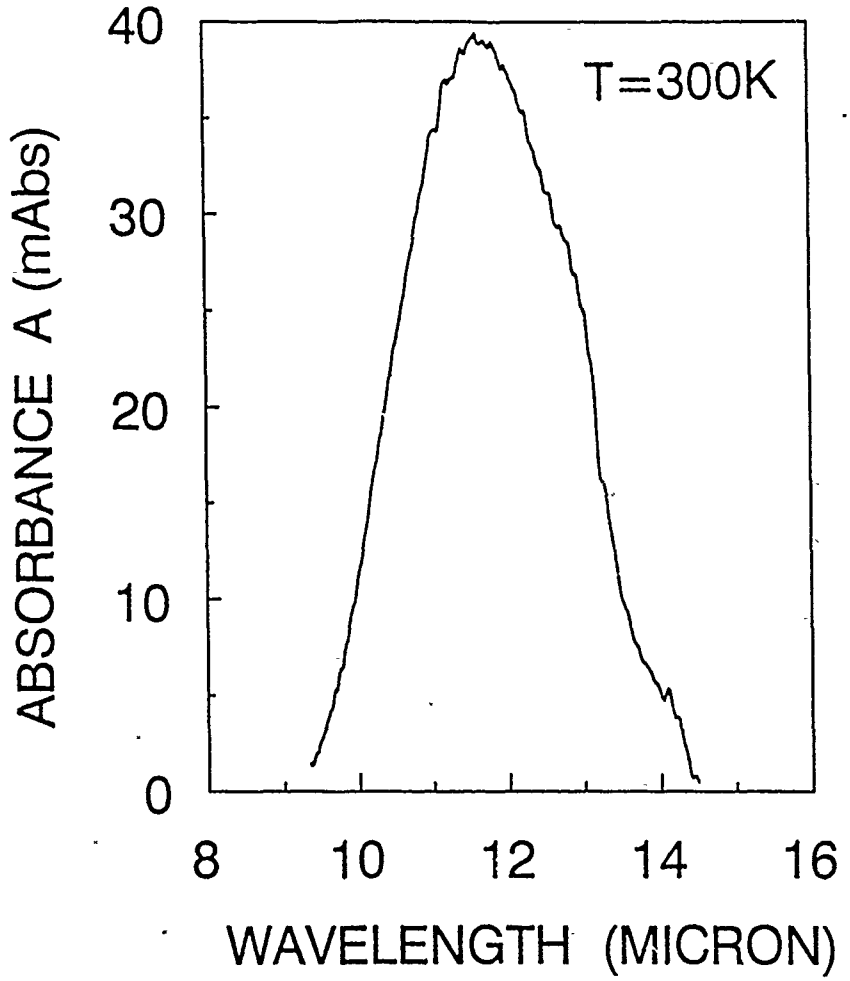

Figure.4 The intersubband absorbance versus wavelength for the SBTM IR detector shown in Fig.1, measured by FTIR spectroscopy at Brewster's angle and at T = 300 K.

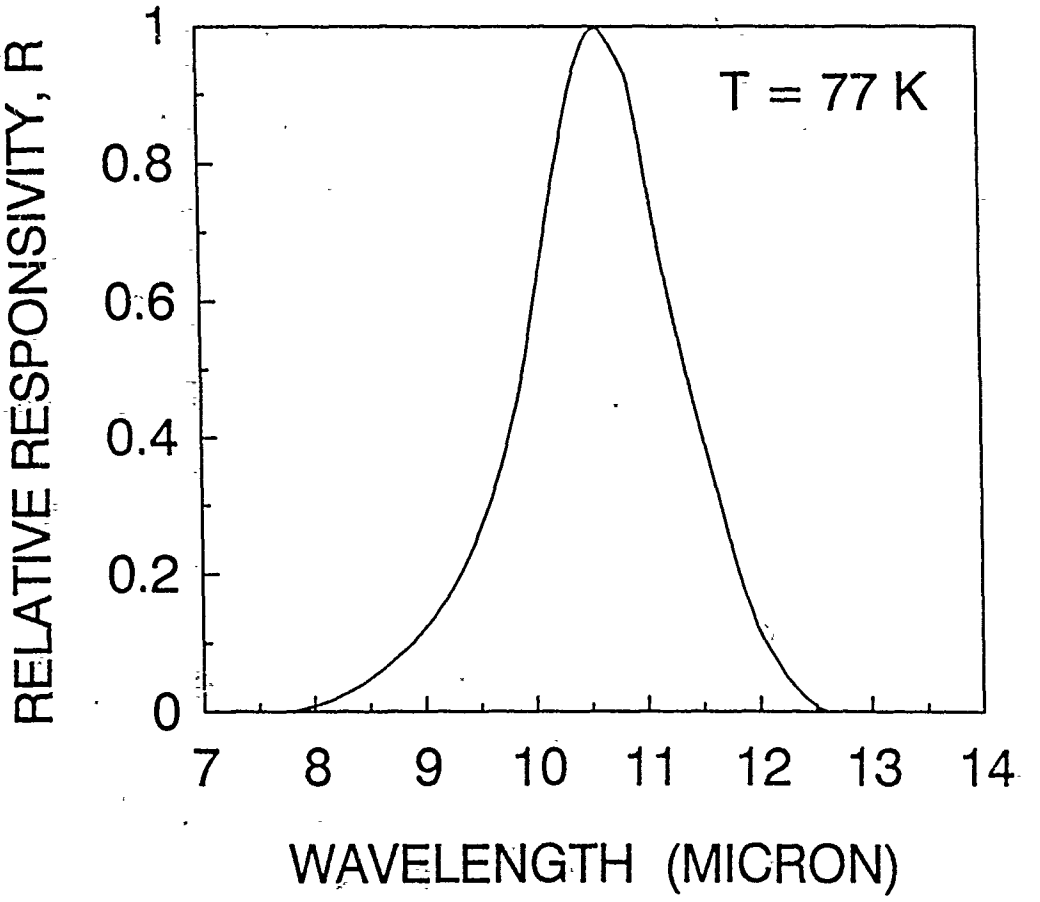

Figure.5 Relative responsivity versus wavelength for the SBTM IR detector shown in Fig.1 , measured at 77 K.

4.2. Largely Enhanced Bound-to-Miniband Absorption in an InGaAs Multiple Quantum Well with Short-Period Superlattice InAlAs/InGaAs Barrier

A strong interest in the development of various high-speed quantum well based- lasers, detectors, and modulators has spurred extensive investigations on the intersubband absorption in quantum wells and superlattices[1-8]. A great deal of work has been carried out in the GaAs/AlGaAs quantum well system[9-17], which shows that the III-V quantum well and superlattice structures are very promising for potential long wavelength (8 - 12 μm) infrared applications. A variety of studies of intersubband absorption have also been conducted in the InAlAs/InGaAs system in the 3 to 5 μm wavelength range by using the bound-to-bound transition[18,19] and bound-to-continuum transition[20], which suggest that the InAlAs/InGaAs, with a large conduction band discontinuity ($\Delta E_c \sim 500mcV$), is an ideal material system for both the mid wavelength infrared (MWIR) and long wavelength infrared (LWIR) applications. There are several other advantages of using the InAlAs/InGaAs in comparison to the AlGaAs/GaAs system. First, the $In_{0.52}Al_{0.48}As/In_{0.53}Ga_{0.47}As$ quantum well has a smaller effective mass ($m^* = 0.042\ m_0$) and hence a larger drift velocity and much shorter transition time, which is essential for many high-speed applications. Second, the higher barrier potential is particularly useful in suppressing the noise due to the electron thermionic emission out of quantum wells and hence reducing the device's dark current. Recent studies[11,13] show that 8 - 12 μm or longer wavelength infrared detectors could also be obtained in a much higher potential quantum well structure by using superlattice barrier structure and resonant tunneling mechanism. A significant improvement in intersubband absorption and thermionic emission property has been successfully demonstrated in the superlattice reinforced bound-to-miniband transition structure[12]. The replacement of bulk barrier region with very short period superlattice multiple layers offers several new properties like reduction of interface recombination, elimination of deep level related phenomena[21], realization of a new type of quantum photocurrent gain ($\sim 10^4$)[22,14], and a significant enhancement of the intersubband absorption.

In this letter we report a detailed study of the long wavelength ($\lambda_p = 10.73\mu$m) infrared intersubband absorption by using a bound-to-miniband transition in the periodically enlarged $In_{0.52}Al_{0.48}As/In_{0.53}Ga_{0.47}As$ multiple quantum well cladded by short-period superlattice barriers. A typical band structure of a bound-to-miniband intersubband excitation used in this experiment is depicted in figure 1. The transition scheme is from the localized ground level E_{EW_1} of the enlarged well (EW) to the resonant-coupled miniband E_{SL_1} of the superlattice (SL). The physical parameters of the quantum wells and superlattices are chosen so that the second level E_{EW_2} of the EW is merged and lined up with the ground level miniband E_{SL_1} of the SL on both sides of the GaAs quantum well to achieve a maximum intersubband absorption strength I_A.

To understand the miniband property and bound-to-miniband transition spectra, theoretical calculations of energy states E_{EW_n}, E_{SL_n} (where n =1, 2, $\cdots$), and transmission coefficient T^*T have been performed for the multiple layer $In_{0.52}Al_{0.48}As/In_{0.53}Ga_{0.47}As$ MQW/superlattice structures by using the multiple-layer transfer matrix method[11]. In this calculation, we have used the $E_g = 0.76$ eV, $m^* = 0.042\ m_0$ for the $In_{0.53}Ga_{0.47}As$, and E_g

= 1.17 eV, $m^* = 0.075\ m_0$ for $In_{0.52}Al_{0.48}As$. The conduction-band discontinuity is taken as $\Delta E_c = 500$ meV. Result is shown in figure 2. It is noticed that a wide and strongly degenerated miniband E_{SL} was formed by using the superlattice structure. The central energy position of the first miniband is at $E_{SL_1} = 138$ meV, and the bandwidth of the first miniband at T ~ 0 K is about $2\Gamma = 40$ meV. The room temperature (T = 300 K) bandwidth is estimated to be $2\Gamma = 60$ meV. The increased bandwidth of the miniband would be helpful to improve the integrated intersubband absorption strength I_A. The peak absorption wavelength can be found from Figure 3 by using the relation $\lambda_p = 1.24/(E_{SL_1} - E_{EW_1} + E_{xch})$, where $E_{SL_1} = 138$ meV, $E_{SEW_1} = 33$ meV, and $E_{xch} = 10$ meV[22,24], which yields $\lambda_p = 10.78$ μm. For comparison, we have also included in Figure 2 the transmission coefficient vs. the potential energy (dashed-line) for a single quantum well with the same barrier width (410 Å) of bulk InAlAs barrier. The result shows that there is a small energy shift in their eigenvalues in the quantum wells as compared to those with superlattice InAlAs/InGaAs barrier (solid line), because the effective barrier heights for the two cases are no longer same. However, a significant difference, as expected, may come from the extremely large transmission coefficient exhibited by the resonant tunneling miniband E_{SL_1} (nearly twenty orders of magnitude larger than that of the bulk barrier), indicating that the miniband is a very efficient charge transport channel.

The $In_{0.52}Al_{0.48}As/In_{0.53}Ga_{0.47}As$ MQW/SL layer structure used in the present study was grown on a lattice matched semi-insulating (100) InP substrate by using the molecular beam epitaxy (MBE) technique. A 1 μm thick Si-doped InGaAs buffer layer with n = $1.4 \times 10^{18}\ cm^{-3}$ was first grown on an InP substrate, followed by the growth of a 20-period of enlarged $In_{0.53}Ga_{0.47}As$ quantum wells (EWs) with a well width of 110 Å and a dopant density of $1.4 \times 10^{18}\ cm^{-3}$. The barrier layer on each side of the EW consists of a 6-period of undoped $In_{0.52}Al_{0.48}As$ (30 Å)/5-period of $In_{0.53}Ga_{0.47}As$ (46 Å) superlattice layers which were grown alternatively with the $In_{0.53}Ga_{0.47}As$ (110 Å wide) quantum wells. Finally, an n^+-InGaAs cap layer of 0.3 μm thick and dopant density of $1.4 \times 10^{18}\ cm^{-3}$ is grown on top of the MQW/SL layer structure.

The infrared absorption of the sample was measured at room temperature using a Perkin-Elmer Fourier transform infrared (FTIR) spectrometer. Since the intersubband resonance is expected to vanish at normal incidence (the selection rule requires a component of the incident electric field normal to the quantum well interfaces), the sample was oriented at the Brewster's angle[2] ($\theta_B \sim 74.5°$) to maximize the intersubband absorption under surface illumination. Figure 3 shows the result of a room temperature absorption spectrum measurement. The peak absorbance A = $-log_{10}$[transmission] was found to be 39.5 mAbs , which corresponds to a transmission reduction of $\Delta T/T = 9$ %. The absorption peak is at $\lambda = 10.73\mu$m and the spectral linewidth (full width at half-maximum) of this transition is equal to 500 cm^{-1} (~ 62 meV), in very good agreement with theory.

The intersubband absorption spectrum cited above corresponds to the transitions between the localized ground state E_{EW_1} to the 'global' miniband state E_{SL_1} which consist of numerous eigenstates of the superlattice (SL). Their energy levels are so closely packed together that they become a broad and highly-degenerated energy state—miniband. The total ab-

sorption is due to the net contribution from all the transitions between the first bound state and each sub-miniband state. Therefore, the integrated intersubband absorption strength I_A can be written as[2,25]

$$I_A = \int\int A(\lambda, E) dE d\lambda = \sum_{E_i} \sum_{E_f} n_s N \frac{e^2 h}{4\epsilon_0 m^* c} \frac{f}{n^2\sqrt{n^2+1}} \tag{4}$$

$$\simeq Q n_s N \frac{e^2 h}{4\epsilon_0 m^* c} \frac{f}{n^2\sqrt{n^2+1}} \tag{5}$$

The oscillator strength f is defined by

$$f = (4\pi m^* c/\hbar\lambda) < z >^2 \tag{6}$$

where λ is the transition wavelength, $A(\lambda, E)$ is the spectral and energy dependence of intersubband absorbance, E_i and E_f denote the quantized energy levels for the initial and final states, $n_s = 1.54 \times 10^{12}\ cm^{-2}$ is the two-dimensional electron sheet density, $m^* = 0.042 m_o$ is the electron effective mass, N=20 is the number of enlarged quantum wells, n = 3.6 is the refractive index of $In_{0.53}Ga_{0.47}As$ in the infrared range of interest, Q is the effective number of states within the miniband which contributes to the total intersubband absorption. Considering the fact that the effective overlapping and coupling of the electron wavefunction between the enlarged quantum well and the superlattice mainly occurs within the nearest regions ($\sim$ 120 Å) adjacent to either side of the enlarged quantum well, the effective number of miniband Q is found to be approximately 4.7 for the present study. From figure 3, by integrating the area under the intersubband absorption spectra, we obtained the integrated absorption strength I_A = 19.5 Abs-cm^{-1} . Substituting them into Eqs.(2) and (3), we obtained f = 0.73 and $< z >$ = 23.9 Å which agreed reasonably well with our theoretical values f = 0.71 and $< z >$ = 23.6 Å.

Figure 4 shows the calculated integrated absorption strength I_A of the bound-to-miniband transition as compared to the single bound-to-bound transition in the conventional quantum wells with uniform bulk barriers. As expected, the integrated absorption strength I_A increases almost linearly with the well width L_z. By incorporating the superlattice miniband, nearly five fold improvement in the integrated absorption strength I_A has been achieved in the present 110 Å quantum well structure, which indicates that a wide quantum well and a broad miniband are essential to obtain large intersubband absorption. We have also calculated the range of photon energies which could be operational in the $In_{0.52}Al_{0.48}As/In_{0.53}Ga_{0.47}As$ system and found that a broad range of photon absorption from 400 to 100 meV can be covered; corresponding to the interest spectral wavelengths from 3 to 12 μm, in a single lattice-matched material system without having to switch to a different material (e.g., GaAs/AlGaAs) system. These unique properties are important for realizing multiple spectral (multi-color) detectors and high quality image arrays.

In conclusion, we have reported the first observation of intersubband absorption of the bound-to-miniband states transition in a lattice matched $In_{0.52}Al_{0.48}As/In_{0.53}Ga_{0.47}As$ multiple

quantum well/ superlattice heterostructure grown on an InP substrate. The peak intersubband absorbance was found to be A_p = 39.5 mAbs with a peak wavelength centered at λ = 10.73 μm, and the spectral linewidth is measured to be 2Γ = 62 meV at T = 300 K, which are in good agreement with our theoretical calculations. The dependence of the integrated absorption strength I_A on the well width and effective number of miniband was discussed. An extremely large integrated absorption strength I_A = 19.5 Abs-cm^{-1} at the Brewster's angle (74.5°) has been obtained in our present 110 Å enlarged quantum well/superlattice barrier structure at T = 300 K , confirming a broad miniband and a wide quantum well are advantageous for large intersubband absorption. By varying the well width the interesting spectral range λ = 3 - 12 μm can be covered, which may lead to the development of new types of infrared sources, modulators, and detectors.

REFERENCES

1. J. S. Smith, L. C. Chiu, S. Margalit, A. Yariv, and A. Y. Cho, J. Vac. Sci. Technol. B 1, 376 (1983).

2. L. C. West and S. J. Enlash, Appl. Phys. Lett. 46, 1156 (1985).

3. B. F. Levine, K.K. Choi, C.G. Bethea, J. Walker, and R. J. Malik, Appl. Phys. Lett. 50, 1092 (1987).

4. D.D. Coon andR.P.G. Karunasiri, Appl Phys. Lett. 33, 495 (1984).

5. X. Zhou, P.K. Bhattacharya, G. Hugo, S.C. Hong, and E. Gulari, Appl. Phys. Lett., 54, 855 (1989).

6. S.D. Gunapala, B.F. Levine, R.A. Logan, T. Tanbun-Ek, and D.A. Humphrey, Appl. Phys. Lett., 57, 1802 (1990).

7. A. Kastalsky, T. Duffield, S.J. Allen, and J. Harbison, Appl. Phys. Lett. 52, 1320 (1988).

8. P.F. Yuh and K.L. Wang, Appl.Phys. Lett. 65. 4377 (1989).

9. B. F. Levine, C.G. Bethea, G. Hasnain, V.O. Shen, E.Pelve, R.R. Abbott, and S.J. Hsieh, Appl. Phys. Lett. 56, 851 (1990).

10. G. Hasnain, B.F. Levine, S. Gunapala, and [illegible] Chand, Appl. Phys. Lett. 57, 605 (1990).

11. Larry S. Yu, Sheng S. Li, Y.C. Kao, *Proc. Government Microcircuit Applications Conference*, Nov. 6 -8, Las Vegas, Nevada, p. 479 (1990).

12. Larry.S. Yu, S. S. Li, Appl. Phys. Lett. Sept. 9 (1991).

13. Larry. S. Yu, S. S. Li, Y.C. Kao, *Proc. International Electron Devices and Materials Symposium*, Nov. 14 - 16, Hsinchu, Taiwan, 468 (1990).

14. S S. Li, Y.H. Wang, L.S. Yu, S. Zhu, R.M. Park and Y.W. Lin *International Electron Devices and Materials Symposium*, Nov. 14 - 16, Hsinchu, Taiwan (1990).

15. B.F. Levine, G. Hasnain, C.G. Bethea, and Naresh Chand. Appl. Phys. Lett., 54, 2704 (1989).

16. M.A. Kinch and A. Yariv, Appl. Phys. Lett. 55, 2093 (1989).

17. K.W. Gossen and S.A. Lyon, Appl. Phys. Lett., 53, 1027 (1988).

18. B.F. Levine, A.Y. Cho, J. Walker, R.J. Malik, D.A. Kleinman, and D.L. Sivco, Appl. Phys. Lett., 52, 1481 (1988).

19. Hiromitsu Asai and Yuichi K[illegible] Appl. Phys.Lett., 56, 746 (1990).

20. G. Hasnain, B.F. Levine, D.[illegible] A. Cho, Appl. Phys. Lett., 56, 770 (1990).

21. H. Sakaki, M. Tsuchiya, and J. Y[illegible]shino, Appl. Phys. Lett., 47, 295 (1985).

22. F. Capasso, K. Mohammed, A.Y. [illegible], R. Hull, A.L. Hutchinson, Appl. Phys. Lett. 47, 420 (1985).

23. O. Byungsung, J.W. Choe, M.H. F[illegible]ancombe, K.M.S.V. Bandara, and D.D Coo[illegible] Appl. Phys. Lett. 57, 503 (1990).

24. Walter L. Bloss, J. Appl. Phys. 66 (8), 3639 (1989).

25. D. Ahn and S.L. Chuang, Phys. Rev. B 35, 4149 (1987).

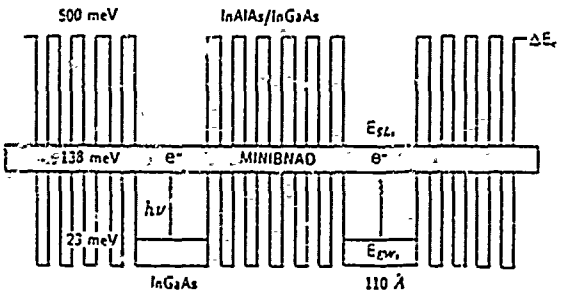

Fig. 1 The bound-to-miniband transition followed by superlattice transport and effective mass filtering.

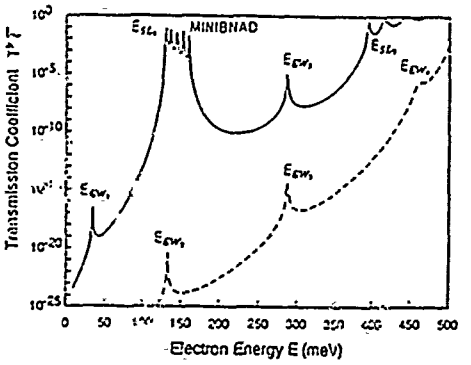

Fig. 3 Calculated transmission T vs. the electron potential energy E (meV) through the superlattice barrier. A highly degenerated miniband state is clearly formed in the superlattice.

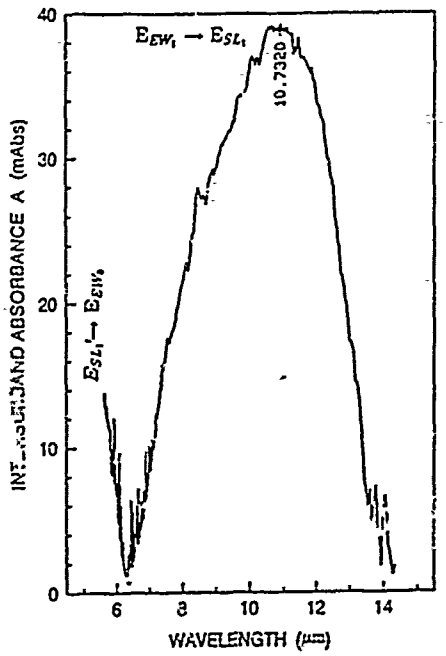

Fig. 2 Measured intersubband absorbance at room temperature vs. infrared radiation wavelength by the Fourier transform infrared (FTIR) spectroscopy at the Brewster's angle.

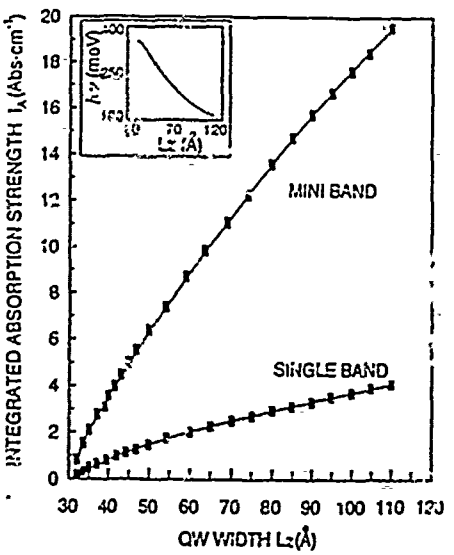

Fig. 4 Enhanced integrated absorption strength I_A for the bound-to-miniband transition with respect to the conventional single bound-to-bound transition.